

The Infrared Counterparts of the Optically Unidentified CDF-S 1Ms Sources¹

Haojing Yan², Rogier A. Windhorst², Huub J. A. Röttgering³, Seth H. Cohen², Stephen C. Odewahn², Scott C. Chapman⁴, and William C. Keel⁵

ABSTRACT

The Chandra Deep Field South (CDF-S) 1Ms exposure produced a catalog of 346 X-ray sources, of which 59 were not visible on the VLT/FORS1 and the ESO-MPI/WFI deep *R*-band images to a limit of $R_{vega}=26.1\text{--}26.7$ mag. Using the first release of the ESO VLT/ISAAC *JHK_s* data on the CDF-S, we identified six of the twelve such objects that were within the coverage of these IR observations. The VLT/FORS1 *I*-band data further confirms that five of these six objects are undetected in the optical. The photometric properties of these six counterparts are compared against those of the optically brighter counterparts of Chandra sources in the same field. We found that the location of these optically brighter Chandra sources in the near-IR color space was bifurcated, with the color of one branch being consistent with that of E/S0 galaxies at $0 \leq z \leq 1.5$ and the other branch being consistent with that of unreddened AGN/QSOs at $0 \leq z \leq 3.5$. The six counterparts that we identified seemed to lie on the E/S0 branch and its extension, suggesting that these X-ray source hosts are mostly luminous E/S0 galaxies ($M_V \sim -20$ mag in AB system) at $1 \leq z \leq 2.5$. On the other hand, some of them can also be explained by AGN/QSOs over a wide redshift range ($0 \leq z \leq 5$) if a range of internal extinction ($A_V = 0\text{--}1$ mag) is allowed. However, the later interpretation requires fine-tuning extinction together with redshift for these objects individually. If they are indeed AGN/QSOs, the most luminous of

¹Based on observations made with the European Southern Observatory telescopes obtained from the ESO/ST-ECF Science Archive Facility.

²Department of Physics and Astronomy, Arizona State University, Tempe, AZ 85287-1504; Haojing.Yan, Rogier.Windhorst, Seth.Cohen, Stephen.Odewahn@asu.edu

³Leiden Observatory, P. O. Box 9513, 2300 RA Leiden, The Netherlands; rottgeri@strw.leidenuniv.nl

⁴Department of Physics, California Institute of Technology, 1200 E. California Blvd., Pasadena, CA 91125; schapman@irastro.caltech.edu

⁵Department of Physics and Astronomy, University of Alabama, Tuscaloosa, AL 35487; keel@bildad.astr.ua.edu

them is just barely qualified for being a QSO. Finally, we point out that neither high-redshift ($z > 5$) star-forming galaxies nor irregular galaxies at lower redshift can be a viable explanation to the nature of these six counterparts.

Subject headings: cosmology: observations — galaxies: evolution — infrared: galaxies — X-rays: galaxies

1. Introduction

The investigations conducted prior to the launches of Chandra and XMM have speculated that a significant fraction of the X-ray background (XRB) is produced by discrete sources, predominantly AGNs (e.g. Hasinger et al. 1998). With its superb spatial resolution, Chandra resolved nearly 100% of the X-ray background in the 0.5–8.0 keV regime into discrete sources (e.g. Mushotzsky et al. 2000), and thus changed the theme of the XRB study into investigating the nature of the discrete X-ray sources and their constraints on galaxy evolution. With the active optical and infrared follow-ups around the two deepest Chandra fields, Chandra Deep Field North (CDF-N; Brandt et al. 2001b) and South (CDF-S; Giacconi et al. 2002), we have gained extensive knowledge about the faint X-ray source population. It is now generally believed that the majority of these sources are dust-obscured type-II AGNs at $z=0\text{--}2$, while a smaller fraction of them are classic type-I AGNs out to $z \simeq 4$ (e.g., Alexander et al. 2001; Tozzi et al. 2001; Norman et al. 2002; Rosati et al. 2002).

However, a significant number of these X-ray sources are still optically unidentified and thus their nature remains uncertain. Within an $8'.6 \times 8'.6$ area at the center of the CDF-N, the multi-wavelength investigation of Alexander et al. (2001) indicates that fifteen, or about 10% of the total X-ray sources do not have counterparts to a 2σ limit of $I = 25.3$ mag (all magnitudes quoted in this letter are in the Vega system unless otherwise noted). Five out of these fifteen sources, however, have near-IR counterparts on the HK' -band images of Barger et al. (1999). Similarly, Giacconi et al. (2002) concluded that 59, or about 17% of the total X-ray sources in the CDF-S were not optically identified at a limit of $R = 26.0\text{--}26.7$ mag. These facts raise a very natural question: are these optically invisible sources merely the fainter tail of the already identified population, or do they constitute a separate population of their own?

In this letter, we study the nature of the optically unidentified sources in Giacconi et al. (2002), which we shall refer to as “ R -unidentified sources”. We utilize the deep VLT/ISAAC JHK_s and VLT/FORS1 I -band data, both of which are now publicly available from the ESO science archive. The analysis of these data are described in §2, and the IR and I -

band identifications are shown in §3, where we present IR identifications of six such X-ray sources. In §4 we explore the possible nature of these sources based on their optical to near-IR photometric properties. We conclude with a summary in §5.

2. Data Analysis

As part of the supporting observations of the *Great Observatories Origins Deep Survey* (GOODS; Dickinson & Giavalisco 2002) fields, the ESO VLT/ISAAC has imaged a large portion of the CDF-S in J , H , and K_s -bands (hereafter JHK_s). The first release of these fully processed and stacked data consists of six continuous fields, and covered about 50 $arcmin^2$ at the center of the CDF-S. To further constrain the optical characteristics of the Chandra sources, we also independently reduced the whole set of CDF-S I -band VLT/FORS1 images (3 hours of exposure, ESO Prog. ID. 64.O-0621(A), PI Gilmozzi) retrieved from the ESO science archive. These I -band data, consisting of four slightly overlapped fields, extend $\sim 150 arcmin^2$ and fully cover the area that the VLT/ISAAC has imaged in the JHK_s . The photometry on both the JHK_s data and the I -band data was done by using the SExtractor routine of Bertin & Arnouts (1996).

For each ISAAC field, the JHK_s images were combined into a master stack, which was then used for extracting sources and defining apertures. While the photometry was performed on the individual passbands, a same aperture defined from the master stack was used for a given source in each passband (i.e., “matched-aperture photometry”). For source detection, we used a 5×5 Gaussian smoothing kernel with the FWHM of 2.5 pixels, which is approximately the same as the FWHM of a point source PSF ($\sim 0.5''$) on the master stack. We set 1.5σ as the detecting threshold, and required at least 5 connected pixels above the threshold for a source to be detected. As the vast majority of the sources are extended, we used total magnitude (corresponding to the *mag-auto* option in SExtractor) for the photometry on the individual passbands. The zeropoints recorded in the image headers were used to convert counts into Vega magnitudes.

We assessed the JHK_s limits in the following way. The representative error reported by SExtractor was used to calculate the S/N of each extracted source, assuming the reported magnitude error (Δm) and the S/N follow the simple relation as $\Delta m = 1.0857/(S/N)$. Only the sources with $S/N \geq 3 \sigma$ were included in the assessment. The source count histogram was constructed for each band, and the magnitudes at which the counts dropped to 50% of the peak values were defined as the survey limits. These numbers are: $J=24.2$, $H=23.4$ and $K_s=23.2$ mag.

Source detection and photometry on the I -band stacks were done in the same manner as in analyzing the ISAAC data excepted that the detection threshold was lowered to 1σ to include as faint sources as possible. As the ESO Imaging Survey (EIS; Arnouts et al. 2002) covered the entire CDF-S, we used their I -band source catalog to calibrated our photometry. We first removed the Galactic extinction ($A_I=0.02$ mag) that they applied to their results, and converted the magnitudes from AB system, which they used, to Vega system by using $I_{\text{vega}} = I_{AB} - 0.48$. The survey limits, derived in the same way as in the ISAAC data analysis, are approximately 25.1 – 25.2 mag accounting for field-to-field variation.

3. Source Cross-matching

Out of the 346 Chandra sources, 77 have their locations falling within the JHK_s coverage, among which twelve are R -unidentified sources. We found that six of these twelve objects could be matched with the JHK_s sources within a matching radius of $1.5''$, all of which were strikingly significant detections (at 3.5 – 9.0σ level) in the K_s -band. After visually examining these matched sources on screen and comparing against the R -band image stamps given in Giacconi et al. (2002), we concluded that these six IR counterparts were real identifications.

We then cross-matched the R -unidentified sources with our I -band images. While 35 of them have their locations within the I -band coverage, only one counterpart was found. This fact further suggests that most of these objects are indeed optically faint. However, the only counterpart, which is also one of the six JHK_s sources, was detected at above 7σ level.

Table 1 lists the positions and the photometric characteristics of the six objects that we identified, together with their X-ray hardness ratios (HR) taken from Giacconi et al. (2002). These six sources are of moderate X-ray fluxes in 0.5–2 kev, with two of them falling toward the faint end ($\sim 8.5 \times 10^{-17}$ erg/s/cm 2). We note that they tend to have negative X-ray hardness ratios. In fact, three of them were detected in the soft channel only ($HR = -1$). Assuming that their underneath X-ray sources are AGNs, it is possible to determine their types based on their HR values. If we use $HR \simeq -0.1$ as the dividing line between low X-ray luminosity (L_X) type-II AGN and high L_X type-I AGN (e.g. Rosati et al. 2002), three of these six Chandra sources are type-I AGNs while the remaining two are type-II AGNs. However, such a division should be used with caution here, as our case is of small number statistics (cf. Fig. 3 of Rosati et al. 2002). The excellent image quality (point source FWHM $\sim 0.5''$ in both IR and I -band) allowed us to at least determine if these sources are of extended morphology. Based on the K_s -band image, where the S/N of the objects is the highest, we determined that three of them were extended sources, and two of them were

point sources. The remaining one is hard to tell because it is close to the K_s -band field edge and its background is much noisier than that of the others.

4. Nature of the Six IR Counterparts

4.1. Possible Candidates

Although these R -unidentified sources could simply be the fainter tail of the brighter objects that have been optically identified, we should not limit our investigation to only this possibility. For this reason, we should consider a wide variety of candidates when exploring the nature of these X-ray source hosts.

As Alexander et al. (2001) argued, it is very unlikely that the objects in the Galaxy could be a major contribution to optically faint X-ray sources. This possibility is even smaller for the CDF-S because it is at high galactic latitude. Thus we consider four types of extragalactic objects as the primary candidates, namely, elliptical galaxies (E/S0), AGNs/QSOs (AGN), irregular galaxies (Irr), and very young galaxies at high redshift ($z > 5$; High-z). We do not include spiral galaxies for the sake of simplicity, as their photometric properties in the I -band and the near-IR lie in between the ellipticals and the irregulars. We compare the six IR counterparts against these four types of candidate ins the IJK_s color space. We consider the redshift range of $5 \leq z \leq 10.5$ for high redshift young galaxies, and $0 \leq z \leq 5$ for all the other three types of candidates. We also consider the effect of internal dust extinction of $A_V=0.1\text{--}3$ mag, following the standard Milky Way extinction law. For the wavelength range shortward of 2000Å, we use the average values of the LMC, SMC and the Galaxy (e.g. Calzetti, Kinney & Storchi-Bergmann 1994).

4.2. Color-Color Diagram Diagnosis

Because five of these six objects are only visible in the three IR passbands, it is not realistic to perform rigorous photometric redshift analysis based on such limited information. At this stage, we chose to use color-color diagrams as our primary diagnostic tools, which are less quantitative but more robust. The invisibility of these sources in the R -band and blueward was used as a consistency check for each of the four possibilities, and was also used as one of the inputs (detailed below) to constrain the rest-frame luminosity of the sources.

We simulated the colors of the candidate objects by using their representative spectral templates. The templates for E/S0 and Irr were taken from Coleman, Wu & Weedman

(1980) with the extension to UV and IR according to Bruzual & Charlot (1993), and the one for AGN was taken from Vanden Berk et al. (2002; using $f_\lambda \propto \lambda^{-0.45}$ to extend its continuum to the near-IR). For young, high redshift galaxies, we used a 0.1 Gyr age, solar metalicity template from Bruzual & Charlot (1993). These rest-frame spectral templates were redshifted in $\Delta z=0.5$ step, and attenuated for the cosmic H I absorption according to Madau (1994). The resulting spectra were then convolved with the system responses, mainly the filter transmission and the detector quantum efficiency, to generate the colors in the AB magnitude system. When considering dust extinction, the colors were adjusted according to the rest-frame spectral range sampled by the relevant passbands. The colors were finally transferred into the Vega system by adopting the appropriate zeropoints (e.g. Waddington et al. 1999).

Fig. 1 shows the $(H - K_s)$ vs. $(J - K_s)$ color-color diagrams in four separate panels for the four cases. The field objects with $S/N \geq 3$ in all three bands are shown as the green dots, and the Chandra sources that have been identified in R -band are shown as the blue squares. The six IR counterparts are plotted with different symbols based on their hardness ratios: the three solid triangles are the ones with $HR = -1$, the two open hexagons that have $-1 < HR < 0.1$, and the open square is the source that has $HR > 0.1$. Their error bars indicate the photometric errors in their colors, which are calculated as the square-root of the quadratic sum of their photometric errors in the corresponding passbands. The unreddened and reddened colors of the simulated objects at different redshifts are plotted in black crosses and solid red squares, respectively (in the case of E/S0, only unreddened colors are shown). For clarity, only the optimal results are plotted for the reddened colors. These optimal reddening values are $A_V = 1.6, 1.0$ and 1.6 mag for Irr, AGN and High-z cases, respectively. A couple of redshifts are marked to indicate the direction along which the color of the simulate objects changes with redshift.

Similarly, Fig. 2 shows the $(H - K_s)$ vs. $(I - K_s)$ color-color diagrams. The High-z case is not included in this figure, because galaxies at $z > 5$ will *drop-out* from the I -band and thus they cannot put meaningful $(I - K_s)$ constraint on those IR counterparts that are also I -band drop-outs. All the legends are the same as in Fig.1, except that the five of the six IR counterparts that were not detected in the I -band are not plotted with error-bars. Instead, we put upward arrows on them to indicate their $(I - K_s)$ color limits.

It is intriguing to note that the location of those optically visible Chandra sources in the IR color space is bifurcated, as can be clearly seen in Fig. 1. The upper branch coincides with the E/S0 track from $0 \leq z \leq 1.5$ while the lower branch seems to be consistent with the AGN track from $0 \leq z \leq 3.5$. This interpretation does not conflict with the investigation on the brighter sources in Rosati et al. (2002; their Fig. 5.). The six objects that we identified

lie on the upper branch and its extension following the E/S0 track up to $z \simeq 2.5$ (see below).

4.3. Comments on Individual Cases

Using the two color-color diagrams and the source brightness, we are able to set stringent constraints on the nature of these six IR counterparts. We comment on the above-mentioned four possibilities individually.

1. *E/S0* From Fig. 1 and 2 it is obvious that the six sources have colors consistent with unreddened E/S0 galaxies at $z=0.5$ – 2.5 , and introducing internal extinction does not improve the fit. Considering the brightness of these objects, this interpretation is also consistent with their invisibility in the *R*-band and blueward. While No. 593 (the lowest triangle in Fig. 1), which was detected in the *I*-band as well, is probably at $z=0.5$, the other five objects are likely at $1.0 \leq z \leq 2.5$. If we use $z=2.0$ as their representative redshift, their averaged rest-frame *V*-band absolute magnitude is $\sim M_V = -20.1$ mag (in AB system), indicating that they are giant ellipticals. In contrast, No. 593 has only $M_V \simeq -16.7$ mag if it is at $z=0.5$, falling in the dwarf elliptical regime.

2. *AGN* While they can reasonably explain the colors of the optically bright Chandra sources, unreddened AGNs at $0 \leq z \leq 5$ cannot produce colors similar to the six sources (see especially Fig. 2). If internal reddening is introduced, the matching will be improved. However, this interpretation involves both the extinction and the redshift as free parameters, and requires both of them be adjusted for each source individually. If the extinction is forced to be fixed, the best fit is obtained with $A_V = 1.0$ mag, which allows three of the six source (open symbols) to be explained, i.e., at $z \simeq 0$ – 1 or $z \simeq 4$ – 5 . If we take the first interpretation for these *three* objects, their absence from *I*-band and blueward means they can only be at $z \simeq 0.8$ – 1.0 to have a reasonable intrinsic luminosity that still qualified for AGNs ($M(3800$ – $4200 \text{ \AA}) \sim -18$ to -19 mag after de-reddening). If the later interpretation is real, on the other hand, their absolute magnitudes make them fall in the low-luminosity end of QSOs ($M(3800$ – $4200 \text{ \AA}) \sim -23$ to -24 mag after de-reddening). The cumulative QSO surface density inferred from this interpretation (2–3 in 50 arcmin^2) is consistent with the QSO luminosity function extrapolated from that is known at lower redshifts (e.g. Boyle et al. 2000). Particularly, we noted that No. 593 did not fit in this interpretation no matter how the extinction and the redshift were adjusted.

3. *Irr* Similar to the AGN case, the colors of unreddened irregular galaxies match the optically bright Chandra sources but cannot match those of the six *R*-unidentified sources. Introducing internal reddening cannot solve the problem, as Fig. 2 shows. Thus irregular

galaxies are not likely a viable explanation to the nature of the six sources.

4. *High – z* The colors of unreddened high-z galaxies are not consistent with the six sources. Fine-tunning internal reddening value can produce a resonable fit either at the redshift range $7.5 \leq z \leq 8.5$ or at $5.0 \leq z \leq 5.2$. The reddening value thus required is $A_V \simeq 1.0$ mag. However, in either case, the cumulative surface density of such galaxies are at least one order of magnitude higher than a reasonable luminosity function would predict (following the same methodology as in Yan et al. 2002). Thus we conclude that this hypothesis is not a viable interpretation either.

5. Summary

We present deep optical and near-IR identifications of the R -unidentified X-ray sources in the CDF-S, using the deep VLT/ISAAC and FORS1 imaging data publicly available from the ESO science archive. Alexander et al. (2001, 2002) did a similar work over a comparable size of area around the CDF-N, who largely focused on the optically faint *but visible sources*. The VLT data that we used reached at least two magnitudes deeper than theirs in the near-IR, and was at least twice as deep in the I -band. More importantly, the three near-IR bands used in this study allow us to further constrain the nature of such sources.

We found six IR counterparts for the CDF-S 1Ms sources that were not optically identified to $R=26.1$ – 26.7 mag, making it possible to carry out spectroscopic study in the future. The X-ray hardness ratio of these six Chandra sources are more negative, opposite to the trend found among the similar, but optically brighter sources in the CDF-N (Alexander et al. 2001). The multi-band photometric properties of these six sources are compared against those of the optically visible Chandra sources in the same field. We found that the location of these optically brighter Chandra sources in the near-IR color space was bifurcated, with the color of one branch being consistent with that of E/S0 galaxies at $0 \leq z \leq 1.5$ and the other branch being consistent with that of unreddened AGN/QSOs at $0 \leq z \leq 3.5$. The six counterparts that we identified seem to lie on the E/S0 branch and its extension, suggesting that these X-ray source hosts are mostly luminous E/S0 galaxies ($M_V \sim -20$ mag in AB system) at $1 \leq z \leq 2.5$. Such luminous ellipticals that host X-ray sources might be similar to those found by Cowie et al. (2001), which are amplified by a foreground cluster. On the other hand, some of these six sources can also be explained by AGN/QSOs over a wide redshift range ($0 \leq z \leq 5$) if various internal extinction ($A_V = 0$ – 1 mag) is allowed. However, the later interpretation requires fine-tuning extinction together with redshift for these objects individually. If they are indeed AGN/QSOs, the most luminous of them is just barely qualified for being a QSO. Finally, we point out that neither high-redshift ($z > 5$)

star-forming galaxies nor irregular galaxies at lower redshift can be a viable explanation to the nature of these six counterparts.

REFERENCES

Alexander, D., et al. 2001, AJ, 122, 2156
———, 2002, AJ, 123, 1149

Boyle, B. J., et al. 2000, MNRAS, 317, 1014

Bertin, E. & Arnouts, S. 1996, A&AS, 117, 393

Brandt, W., et al 2001a, AJ, 122, 1
———, 2001b, AJ, 122, 2180

Bruzual, A. & Charlot, S. 1993, ApJ, 405, 538

Calzetti, D., Kinney, A. & Storchi-Bergmann, T. 1994, ApJ, 429, 582

Cowie, L., et al. 2001, ApJ, 551, L9

Coleman, G., Wu, C.-C. & Weedman, D. 1980, ApJS, 43, 393

Dickinson, M. & Giavalisco, M. 2002, astro-ph/0204213

Giacconi, R., et al. 2002, ApJS, 139, 369

Hasinger, G., et al. 1998, A&A, 329, 482

Madau, P. 1995, ApJ, 441, 18

Norman, C., et al. 2002, ApJ, 571, 218

Rosati, P., et al. 2002, ApJ, 566, 667

Vanden Berk, D., et al. 2002, AJ, 122, 549

Waddington, I., et al. 1999, ApJ, 526, L77

Yan, H., et al. 2002, to be published in ApJ(astro-ph/0208080)

Table 1:

ID ^a	RA & DEC (J2000) ^b	<i>I</i> ^c	<i>J</i> ^d	<i>H</i> ^d	<i>K_s</i> ^d	P/E ^e	HR ^f
79	3:32:38.04 -27:46:26.2	> 25.1	23.21±0.23	21.88±0.17	20.95±0.12	P	-0.42
593	3:32:14.79 -27:44:02.5	24.86±0.18	22.97±0.21	21.66±0.14	21.18±0.13	E	-1.00
221	3:32:08.91 -27:44:24.8	> 25.1	25.08±0.66	22.41±0.21	21.83±0.17	P	-1.00
515	3:32:32.17 -27:46:51.5	> 25.1	24.68±0.76	22.91±0.27	21.90±0.21	E	0.41
561	3:32:22.44 -27:45:43.8	> 25.1	25.73±0.86	23.49±0.38	22.68±0.29	E	-1.00
201	3:32:39.06 -27:44:39.3	> 25.1	24.79±0.58	22.62±0.21	21.52±0.16	...	-0.06

^aSource ID as in Giacconi et al. (2002; their XID).

^bRA and DEC as measured on the *JHK_s* images.

^cThe "auto" magnitude (Kron magnitude) as derived by SExtractor, in Vega system.

^dSame as c; aperture used for each source is the same in all these three bands.

^ePoint (P) or extended (E) source, based on the *K_s*-band images, on which a point source has a FWHM of only $\sim 0.5''$.

^fX-ray hardness ratio (HR), defined as (H-S)/(H+S), where H and S are the counts in the hard and soft channel, respectively. Values are taken from Giacconi et al. (2002).

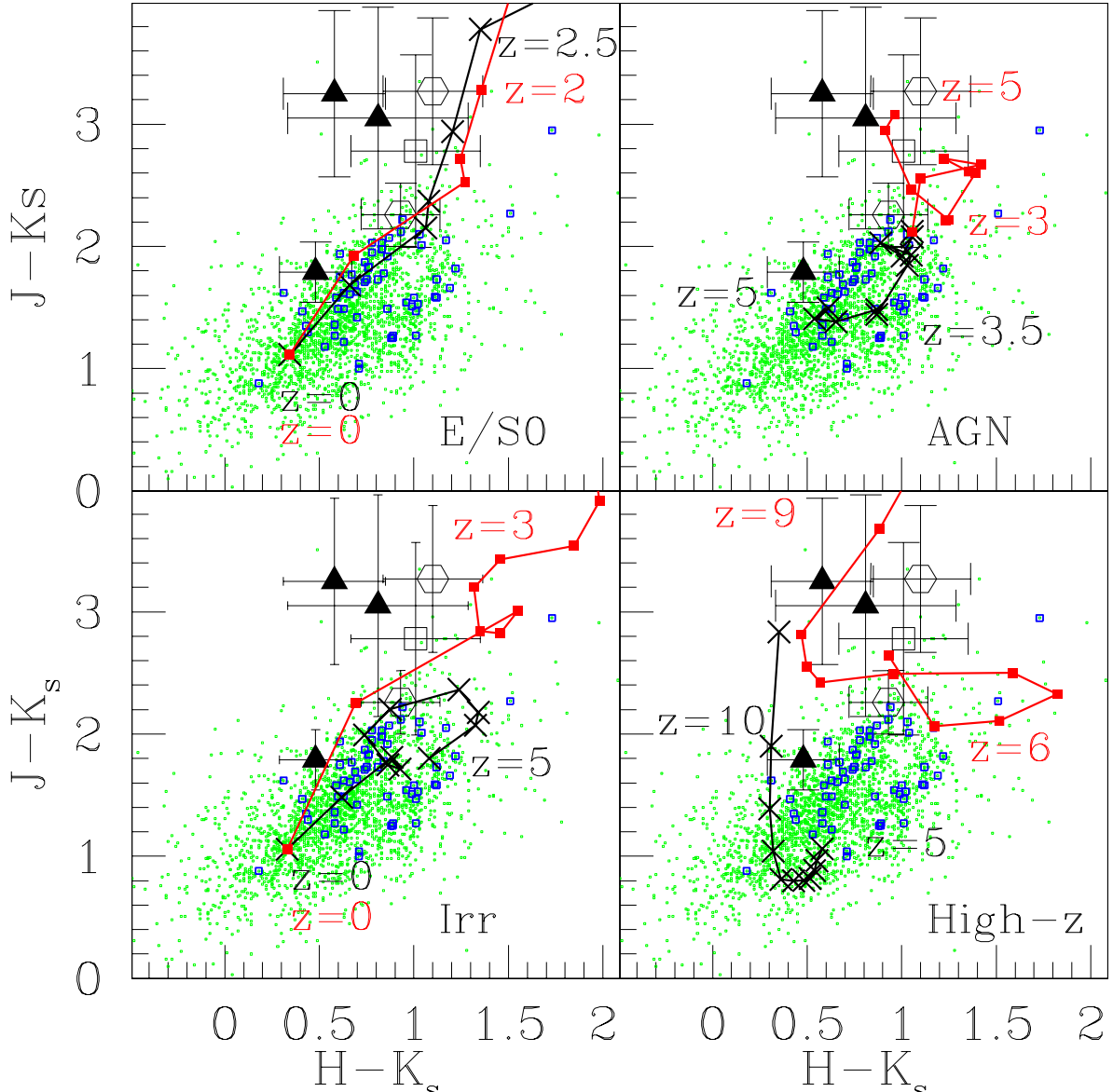


Fig. 1.— $(H - K_s)$ vs. $(J - K_s)$ color-color diagram as the diagnostic tool of the source nature. The green dots are the field objects. The open blue squares are the optically bright Chandra sources, whose locus shows clear bifurcated structure. The large symbols with error bars are the six R -unidentified Chandra sources that were identified in the IR: the three solid triangles are the sources with $HR=-1$, the two open hexagons are the ones with $HR<-0.1$, and the open square is the source d with that has $HR>-0.1$. Their colors are compared against the simulated colors of four types of candidate in separate panels. The redshift ranges considered are $0 \leq z \leq 5$ for E/S0, Irr and AGN/QSO, and $5 \leq z \leq 10.5$ for High-z. Dust extinction ranging from $A_V=0.5$ to 3.0 mag is also considered. For clarity only the cases with the optimal amount of dust extinction are shown ($A_V = 0.5$ mag for E/S0, $A_V = 1.0$ mag for AGN/QSO and High-z, and $A_V = 1.6$ mag for Irr). The unreddened colors of these simulated objects are shown as black crosses, while their reddened colors are shown as filled red squares. A couple of redshifts are also marked (in both unreddened and

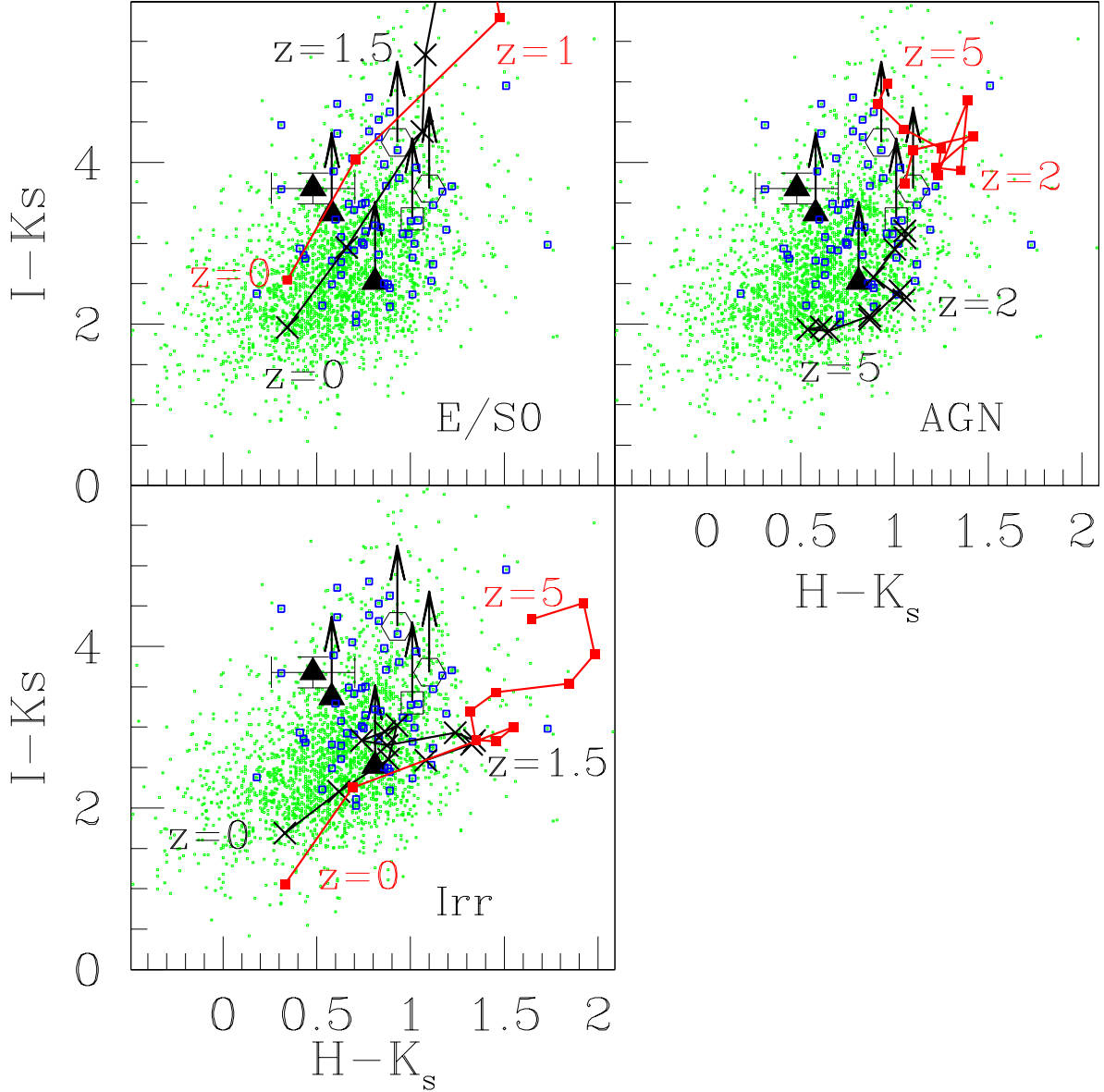


Fig. 2.— Same as Fig. 1, but for the $(I - K_s)$ vs. $(H - K_s)$ color-color diagram. The High-z case is not shown, as it cannot put further constraint on the $(I - K_s)$ of the six IR counterparts (see text). The arrows indicate the lower limit of the $(I - K_s)$ color for the five objects that were not detected in the I -band. Very importantly, the case of irregular galaxies does not pass this test because the $(I - K_s)$ of such objects are not consistent with the colors of the IR counterparts, even considering the effect of dust extinction.